Journal of Molecular Structure 1222 (2020) 128937

Contents lists available at ScienceDirect

Journal of Molecular Structure

journal homepage: www.elsevier.com/locate/molstr

Growth, Z-scan and density functional theoretical study for investigating the nonlinear optical properties of guanidinium L-glutamate for optical limiting applications

Rejeena V. Rajan[a,b], Merin George[a], D.R. Leenaraj[c], Reena Ittyachan[d], D. Sajan[a,*], G. Vinitha[e]

[a] Centre for Advanced Functional Materials, Postgraduate and Research Department of Physics, Bishop Moore College, Mavelikara, Alappuzha, Kerala 690110, India
[b] St. Cyril's College, Department of Physics, Vadakkedathukavu P.O., Kilivayal, Adoor, Pathanamthitta 691529, India
[c] Centre for Molecular and Biophysics Research, Department of Physics, Mar Ivanios College, Thiruvananthapuram 695 015, Kerala, India
[d] Department of Physics, Sacred Heart College, Chalakudy, Kerala, 680307, India
[e] Division of Physics, School of Advanced Sciences, Vellore Institute of Technology (VIT), Chennai 600127, India

ARTICLE INFO

Article history:
Received 12 February 2020
Revised 16 July 2020
Accepted 18 July 2020
Available online 19 July 2020

Keywords:
Nonlinear optics
Z-scan
Optical limiting
Dft

ABSTRACT

A novel semi-organic single-crystal exhibiting third order optical nonlinearity was grown by the method of slow evaporation. Single crystal X-ray diffraction technique (XRD) was employed to confirm the crystal structure and powder XRD was used to determine the cell parameters. The sample was characterized using FT-IR, FT-Raman and UV–visible absorption and analysed with density functional theory (DFT) calculations. The detailed interpretation of the vibrational spectra has been carried out using normal coordinate analysis (NCA) through the scaled quantum mechanical force field methodology. The red shifting of NH stretching wavenumbers, both the observed and calculated, affirm that N–H.....O type bonds are present in GuLG. The Natural Bond Orbital (NBO) analysis also points to a strong intermolecular N–H....O hydrogen bond. Thermal stability of the crystal was studied making use of the TG/DTA technique. The third-order nonlinearity studies, along with the optical limiting behaviour were investigated by Z-scan technique using diode-pumped Nd: YAG laser with 50 mW power at 532 nm.H

1. Introduction

Nonlinear optical (NLO) materials are very much essential in areas like laser frequency conversion, optical communication and optical data storage [1–4]; but their properties are not up to the mark to be efficient for these applications. In order for them to be useful, NLO materials having properties such as high optical susceptibility (χ) and laser damage resistance, appropriate transparency cut off wavelengths, good thermal stability and mechanical performance are required. A possible way to counteract this shortcoming is to explore and design novel NLO materials. A lot of inorganic and organic materials with useful physical and chemical characteristics have thus been studied [5–9]. Studies reveal that normal inorganic NLO materials are suitable for growing large size crystals due to their good mechanical properties and thermal stability. Organic crystals, on the other hand, are not suitable for growing large size crystals [13] due to their poor mechanical strength and thermal stability although they possess fast response times, high optical susceptibilities and high laser damage threshold [10–12]. Semi organic crystals are of interest due to their high damage threshold, wide transparency range, less deliquescence, excellent non-linear optical coefficient, low angular sensitivity and exceptional mechanical properties [14,15]. Guanidinium based organic compounds with π-bonds show good nonlinearity which aid molecular engineering for optoelectronic applications. Recently, many guanidinium based compounds showing nonlinear optical behaviour, including guanidinium 4-hydroxybenzoate [16], guanidinium tetrafluoroborate [17], bis(guanidinium) hydrogen phosphate monohydrate [18], guanidinium 3-nitrobenzoate [19], guanidinium chlorochromate [20], guanidinium carbonate [21], guanidinium L-glutamate [22], zinc guanidinium sulphate [23] guanidinium perchlorate [24], guanidinium cinnamate [25] and guanidinium propionate [26], have been reported. This paper reports the growth and characterization of guanidinium L-glutamate (GuLG),

* Corresponding author:
E-mail address: drsajanbmc@gmail.com (D. Sajan).

https://doi.org/10.1016/j.molstruc.2020.128937
0022-2860/

aided by density functional theory, to elucidate the correlation between the structural features and third order nonlinear optical response and hydrogen bonds, and static and dynamic hyperpolarizability emphasizing the role of intramolecular charge transfer (ICT) mechanism.

2. Experimental and characterization techniques

The title compound GuLG was synthesized [27] from commercially available guanidine carbonate (Sigma Aldrich) and L-Glutamic acid (Alfa-Aesar) taken in a molar ratio 0.5: 1.0 in water–acetone (1:2) by slow evaporation technique at room temperature. Pure salt was obtained though successive recrystallization, which was then dissolved in water–methanol (1:1) solvent to harvest transparent, colourless single crystals of GuLG with dimension $7 \times 3 \times 2$ mm^3 (Fig. 1(a)) within 3–4 weeks.

The grown crystal of GuLG was characterized using X-ray diffraction technique using Bruker AXS Kappa APEX II single crystal X-ray diffractometer with MoKα (λ = 0.710 Å) at room temperature and the crystal structure and lattice parameter values were calculated. The ^{1}H and ^{13}C NMR spectra of GuLG were measured in water–acetone solvent using Bruker 400 MHz Spectrometer. Fourier transform infrared (FTIR) spectrum was recorded in methanol solvent in the range 4000–400 cm^{-1} at 2 cm^{-1} resolution using Thermo Nicolet, Avatar 370 spectrometer. FT-Raman spectrum was recorded by employing BRUKER RFS 27: Stand-alone FT-Raman Spectrometer with 2.0 cm^{-1} resolution. UV–visible spectrum was recorded in the range of 200–800 nm using JASCO V-770 instrument in methanol solvent. The thermal characteristic of the Guanidinium L-glutamate (GuLG) crystals were studied by TG-DTA method in the 303 K to 773 K range at 275 K/min heating rate in the nitrogen atmosphere using Netzsch STA 449F3 simultaneous thermal analyser system to determine the thermal stability of the grown crystals.

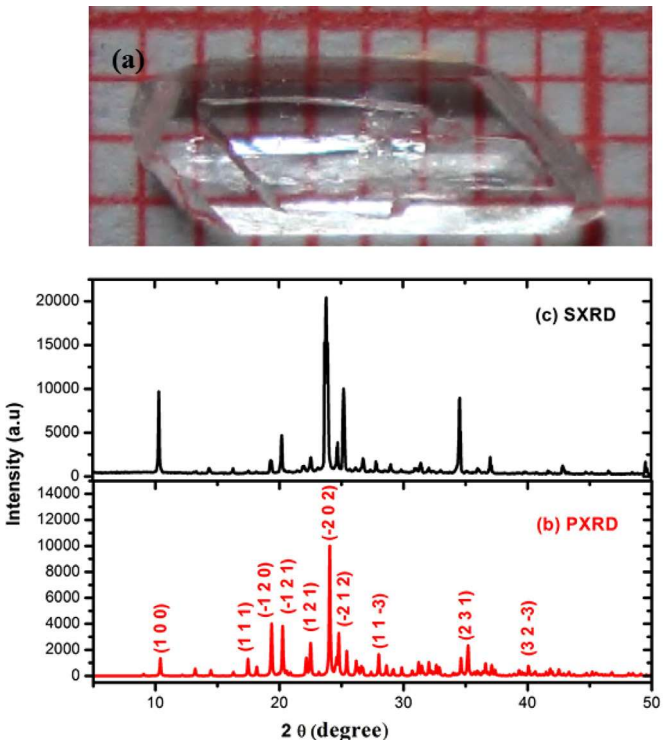

Fig. 1. (a) Phonograph of grown GuLG single crystal. (b) The PXRD data of GuLG (c) Simulated from the SXRD data of GuLG (Ref. [27])) using the Mercury 3.8 program (Ref. [36])).

3. Computational details

The computations were performed with Gaussian '09 program package [28]. The geometry optimization and vibrational wavenumber calculations of GuLG was carried out by employing hybrid functional Becke's three- parameter Lee-Yang-Parr correlation functional (B3LYP) at 6–311++*G*(d) levels of theory, which can provide reliable results for energy data [29–31]. The atomic coordinates for calculations were obtained from the X-ray data [27]. First, the geometry optimization was performed using DFT with the B3LYP correlation functional. The equilibrium geometry corresponding to the true minimum on the potential energy surface (PES) has been obtained by solving self-consistent field equation iteratively. At the optimized structure of GuLG, no imaginary frequency modes were obtained, proving that a true minimum on the potential energy surface was found. The energy is minimized with respect to all geometrical parameters without any constraints and then the geometrical optimization is determined.Harmonic vibrational wavenumbers were calculated using analytic second derivates to confirm the convergence to minima on the potential surface and to evaluate the zero- point vibrational energies (ZPVE). The MOLVIB program version 7.0 written by Sundius [32,33] was employed to perform normal coordinate analysis to obtain full description of molecular motions of the normal modes. Natural bond orbital (NBO) analysis and natural population analysis (NPA) were carried out using NBO 3.1 program [34] of Gaussian '09. Using crystallographic information file, the Hirshfeld surface and two-dimensional finger print plots of the compound were generated by *CrystalExplorer17.5* program [35]. Static and dynamic hyperpolarizabilities were calculated using CAM-B3LYP with 6–311++*G* (d,p) basis set. The electronic absorption and excitation in the crystal were studied theoretically using 6–311++*G* (d,p) in PCM-TD-DFT approach.

4. Results and discussion

4.1. Powder X-ray diffraction analysis

GuLG crystallizes in monoclinic crystal system with non-centrosymmetric space group $P2_1$. XRD analysis reveals the unit cell parameters of GuLG crystal to be a = 8.7785 (6) Å, b = 10.862 (8) Å, c = 10.043(9), β = 104.564°, V = 931.36(3) Å^3, Z = 4, which are found to be similar to reported values [27]. Powder X-ray diffraction (PXRD) pattern has been compared with simulated single crystal X-ray diffraction pattern (SXRD) of GuLG and h,k,l values have been indexed using Mercury 3.8 software [36]. The simulated and experimental XRD patterns are found to agree with each other and are shown in Fig. 1(b) and 1(c). The GuLG crystals have a well-developed morphology with several habit faces. The spiky peaks on a specific 2θ angle confirm the crystalline nature of the grown crystal and the absence of solvent incorporation.

4.2. Optimized geometry

The optimised molecular structure of GuLG simulated with DFT is shown in Fig. 2. Selected geometrical parameters (bond length, bond angle, torsional angle) with XRD data [27] are given in Table-S1 (*Supplementary Information*) for comparison (CCDC N0: 797,855) and the linear regression analysis shown in Fig. 3, with R^2 values of 0.9453 and 0.9200 for the fit of bond lengths and bond angles respectively. The minor deviations in the calculated values of various parameters from the experimental values are due to the interactions inside GuLG. The stabilized structure reveals that the GuLG asymmetric unit is formed by intermolecular N–H···O hydrogen bond between two independent guanidinium cations and two independent L-glutamate anions. The intermolecular hydrogen

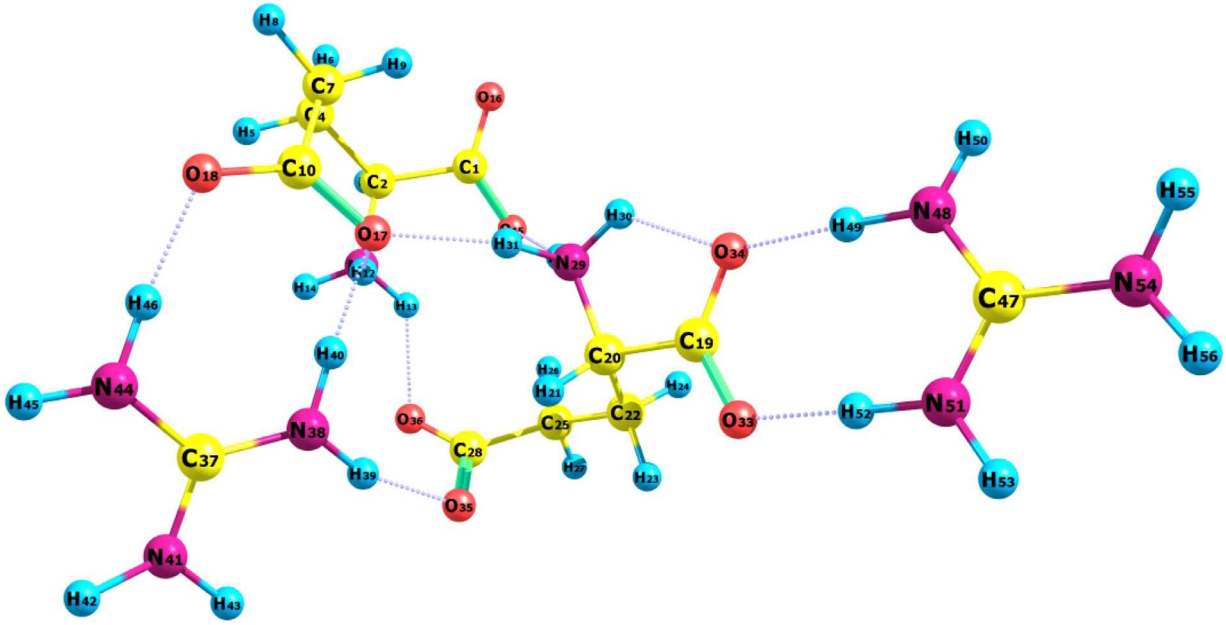

Fig. 2. Optimized molecular structure of GuLG.

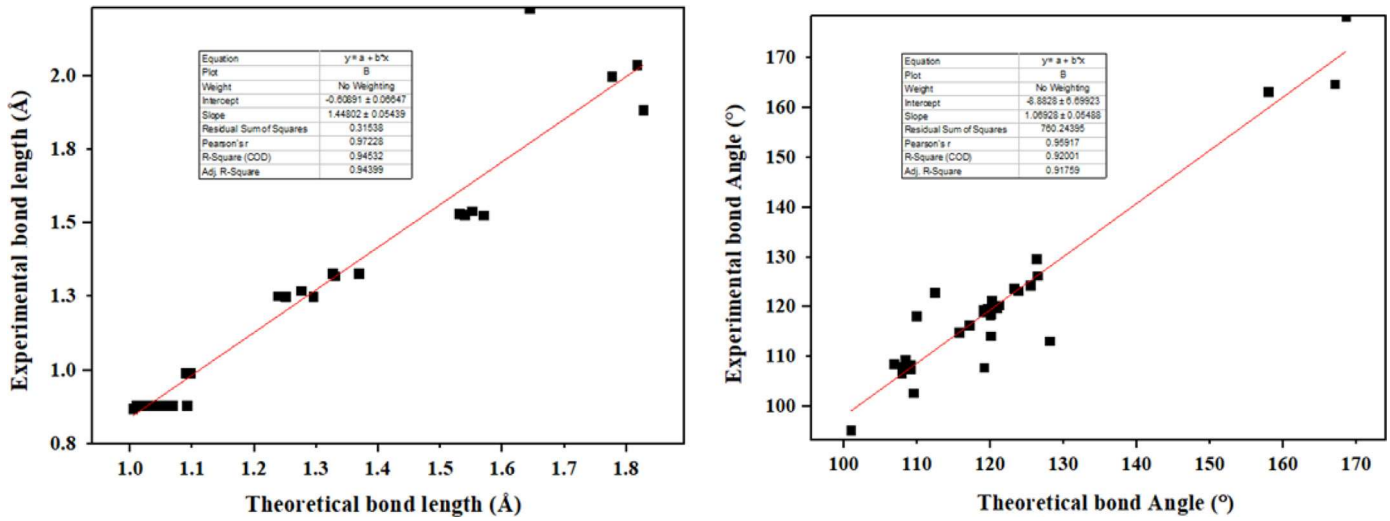

Fig. 3. Linear Regression for bond parameters of GuLG.

bonds N_{11}–H_{13}···O_{36}, N_{29}–H_{31}···O_{17}, N_{29}–H_{32}···O_{15}, N_{38}–H_{39}···O_{35}, N_{38}–H_{40}···O_{17}, N_{44}–H_{46}···O_{18}, N_{48}–H_{49}···O_{34}, N_{51}–H_{52}···O_{33} and the intramolecular hydrogen bonds N_{11}–H12···O_{17} and N_{29}–H_{30}···O_{34} are seen to enhance the corresponding N–H bond lengths. The considerably low values of H_{12}···O_{17}, H_{13}···O_{36}, H_{30}···O_{34}, H_{31}···O_{17}, H_{32}···O_{15}, H_{39}···O_{35}, H_{40}···O_{17}, H_{46}···O_{18}, H_{49}···O_{34} and H_{52}···O_{33} distances which are found to be 1.823, 1.980, 1.940, 1.849, 1.703, 1.665, 1.766, 1.818, 1.645 and 1.602 Å, respectively, when compared to the Van der Waals radii 2.72 Å, suggest the formation of H-bonds. The bond lengths of C_1–O_{15} (1.275 Å), C_{10}–O_{17} (1.295 Å), C_{19}–O_{34} (1.272 Å) and C_{28}–O_{35} (1.273 Å) are slightly larger than that of C_{10}–O_{18} (1.250 Å), C_{19}–O_{33} (1.257 Å) and C_{28}–O_{36} (1.262 Å) and they are intermediate between a single C–O bond length (1.308–1.320 Å) and a double *C = O* bond length (1.214–1.224 Å). The predicted bond lengths of the six C–O bonds of the carboxylate group indicate its hybrid structure. Since the six oxygen atoms are involved in hydrogen bonding at the same time, the O_{17}–C_{10}–O_{18}, O_{35}–C_{28}–O_{36} and O_{33}–C–O_{34} bond angles of the carboxylate groups are extended to 396.77 K, 398.41 K and 399.39 K, respectively. The calculated bond lengths predicted for the C_{37}–N_{38}, C_{37}–N_{41}, C_{37}–N_{44}, C_{47}–N_{48}, C_{47}–N_{51} and C_{47}–N_{54} bonds are 1.311 Å, 1.365 Å, 1.352 Å, 1.330 Å, 1.326 and 1.368 Å, respectively, which are in between the lengths of C–N and *C = N* bonds. The result shows that the charge is delocalized over the cation moieties. The predicted torsional angles for N_{38}–C_{37}–N_{41}, N_{38}–C_{37}–N_{44}, N_{41}–C_{37}–N_{44}, N_{48}–C_{47}–N_{51}, N_{48}–C_{47}–N_{54} and N_{51}–C_{47}–N_{54} of guanidinium cation are different to a small extent from the observed values but the sum of these angles around the central atoms (C_{37} and C_{47}) are found to be 633 K in DFT and XRD data.

4.3. NMR analysis

Experimental and theoretical ^{13}C and ^{1}H NMR spectral chemical shift values relative to TMS values are presented in Table -S2 (*Supplementary Information*) and the ^{13}C and ^{1}H NMR spectra are shown in Fig. 4(a) and 4(b). Carbon atom is compared with other heavier atoms mostly localized on the boundary of molecules. Its

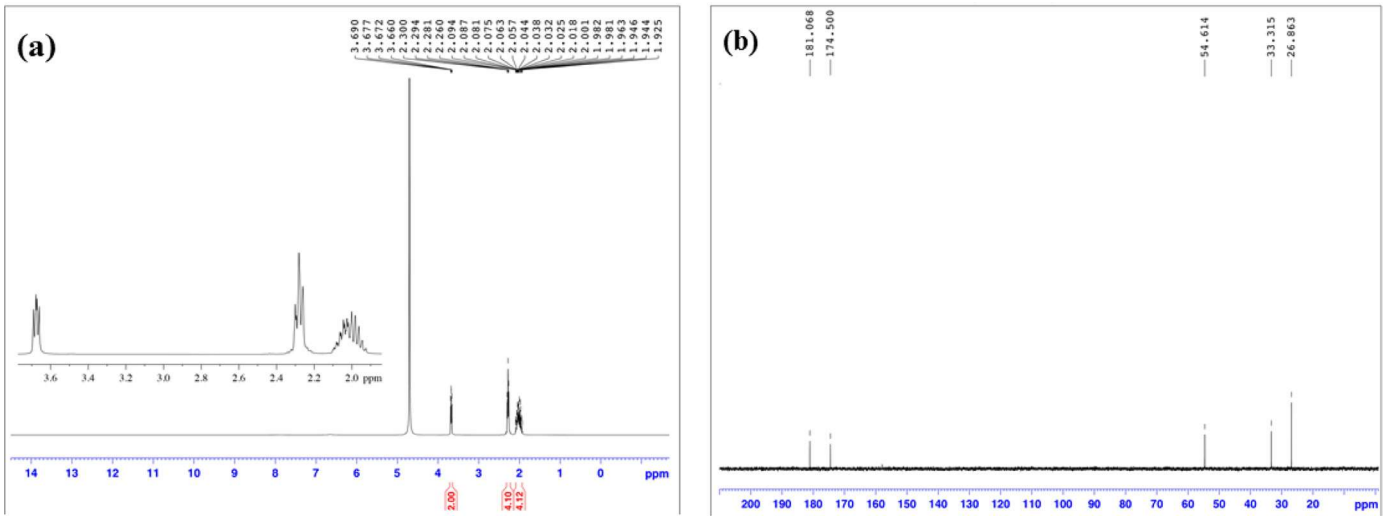

Fig. 4. (a) ^{1}H NMR spectrum of GuLG and (b) ^{13}C NMR spectrum of GuLG.

chemical shifts are influenced by intermolecular interactions. The chemical shift of aromatic carbons is between 100 and 150 ppm [37,38]. Four CO_2 carbons appear at δ174 ppm as quartet and the two L-glutamate carbons appear at δ174 ppm. Influenced by electronegative oxygen and nitrogen atoms, chemical shift values tend to be higher in shift positions. Other ^{13}C NMR are attached with hydrogen atoms. The signals in the 7–9 ppm range are attributed to ring protons, which is normally expected in the 6.9–8.8 ppm region.

4.4. Hirshfeld surface analysis

The Hirshfeld surface of GuLG and its related fingerprint plots in two dimensions were generated using the reported crystallographic information file (CCDC N0: 797,855). Hirshfled surfaces (HS) enable the visualization (2D and 3D plots) of intermolecular interactions making use of distinct colours with varying intensities, to represent their relative strenghts and short or long contacts [39,40]. In Fig. 5a, Hirshfield Surface is plotted over d_{norm}, where contacts with distances equal to the sum of Van der Waals radii are shown in white, while the shorter distance indicating close contact are highlighted in red and the longer ones indicating distinct contacts in blue. In GuLG molecule, the bright red spots appearing near O_{17}, O_{15}, O_{18}, O_{33}, O_{34}, O_{35}, O_{36},H_{12}, H_{13}, H_{30}, H_{31}, H_{32}, H_{39}, H_{40}, H_{46}, H_{49}, and H_{52} indicate that they act as donors and acceptors respectively in the major N–H···O and C–H···O hydrogen bonds. The overall two-dimensional finger print plot, Fig. 5b, and those delineated into H···H, C···H/H···C, N···H/H···N and O···H/H···O contacts are illustrated in Fig. 5c, along with their relative contributions to the HS. The most significant interaction is O···H which contributes 47.7% to the overall crystal packing resulting from a large amount of close interatomic O···H/H···O contacts seen in figure. The O···H/H···O interactions represented by the spikes in the bottom right and left region point out the possibility of hydrogen atoms being in contact with oxygen atoms to form a two-dimensional molecular frame work. The contributions from the other intermolecular contacts to the HS are as follows: H···H (38%), N···H/H···N (7%) and C···H/H···C (5.6%). These intermolecular interactions in GuLG contribute to its nonlinear behaviour.

4.5. Natural bond orbital analysis

The NBO analysis has been employed to study the distribution of electrons across orbitals of anions and cations through intermolecular hydrogen bonding due to the proton transfer and charge transfer or hyper conjugative interactions in the GuLG molecule. Table 1 shows the second-order perturbation energy $E^{(2)}$ determined from B3LYP 6–31++G(d) calculations, which throws light on donor-acceptor delocalization in the molecule. The interaction energy $E^{(2)}$was subtracted from the standard second-order pertur-

Table 1 S
-order perturbation theory analysis of Fock matrix in natural bond orbital basis.

Donor (i)		Acceptor (j)		E(2)[a] kcal/mol	E(j)-E(i)[b] (a.u.)	F(i,j)[c] (a.u.)
NBO	Occupancy	NBO	Occupancy			
Intermolecular hydrogen bonding Interactions						
n1(O_{15})	1.94505	σ^*(N_{29}–H_{32})	0.06963	14.39	1.07	0.111
n1(O_{17})	1.93035	σ^*(N_{29}- H_{31})	0.04277	11.99	1.11	0.104
		σ^*(N_{38}- H_{40})	0.06286	8.44	1.17	0.089
n1(O_{18})	1.96003	σ^*(N_{44}–H_{46})	0.05639	6.61	1.10	0.077
n1(O_{33})	1.95365	σ^*(N_{51}–H_{52})	0.10102	9.64	1.03	0.090
n1(O_{34})	1.94658	σ^*(N_{48}–H_{49})	0.08640	10.96	1.09	0.098
n1(O_{35})	1.95759	σ^*(N_{38}- H_{39})	0.08547	8.14	1.06	0.084
n1(O_{36})	1.96866	σ^*(N_{11}- H_{13})	0.04148	2.73	1.04	0.048
Intramolecular hydrogen bonding Interactions						
n1(O_{17})	1.93035	σ^*(N_{11}- H_{12})	0.05202	12.92	0.66	0.089
n1(O_{34})	1.94658	σ^*($N2_{9}$- H_{30})	0.03228	4.23	1.06	0.060

[a] E(2) means energy of hyperconjugative interactions.
[b] Energy difference between donor and acceptor i and j NBO orbitals.
[c] F(i,j) is the Fock matrix element between i and j NBO orbitals.

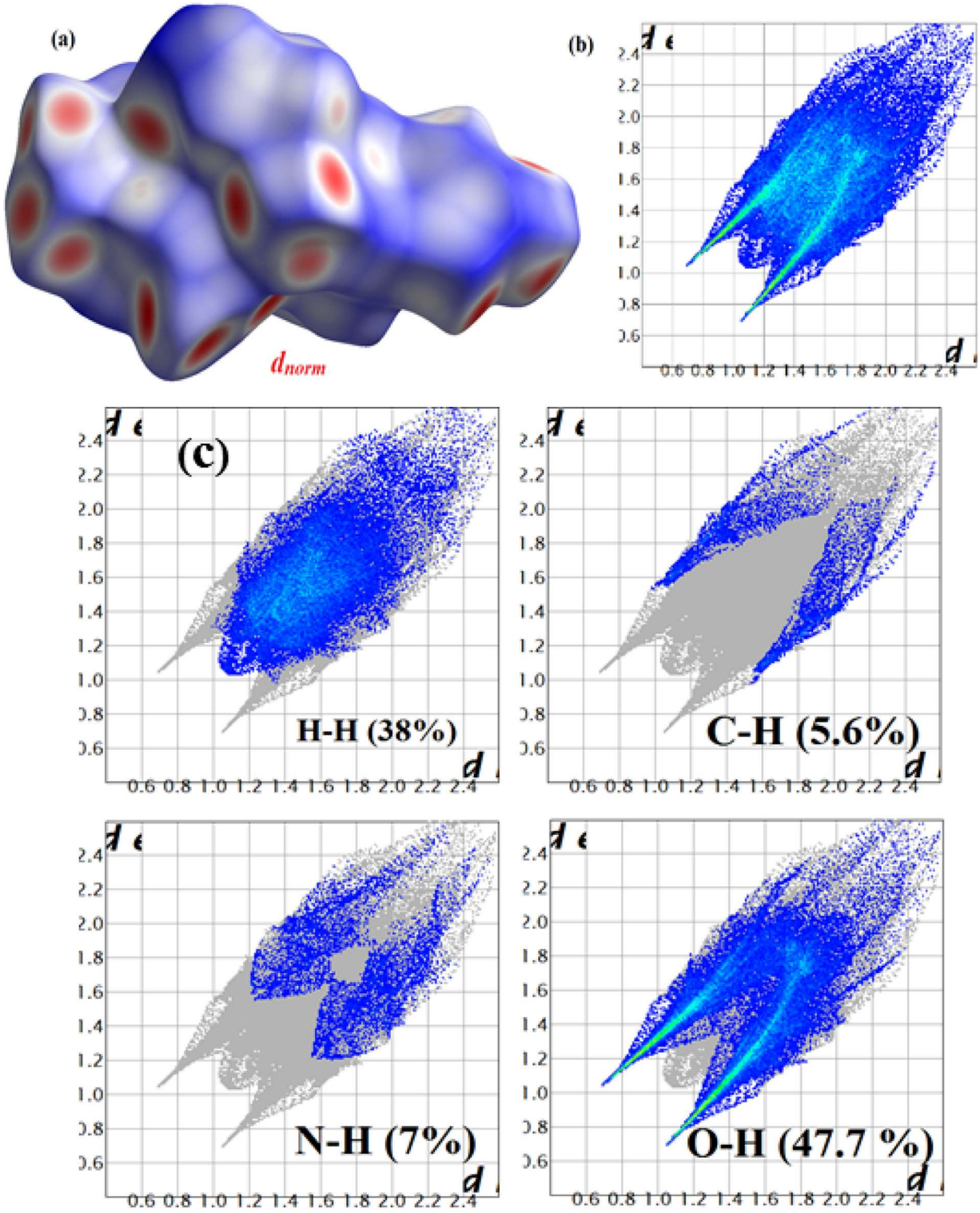

Fig. 5. (a) Hirshfeld*dnorm* surfaces (b) full fingerprint for GuLGmolecule (c) Relative contributions to the percentage of Hirshfeld surface area for the various intermolecular contacts in the GuLG molecule.

bation approach [41].

$$E^{(2)} = -n_\sigma \frac{\langle \sigma | F | \sigma * \rangle^2}{\varepsilon_{\sigma^*} - \varepsilon_\sigma} = -n_\sigma \frac{F_{ij}^2}{\Delta E} \quad (1)$$

Where $\langle \sigma | F | \sigma^* \rangle^2$ or F_{ij}^2 is the KS matrix (Fock matrix) element between i and j NBO orbitals, ε_σ *and* ε_{σ^*} are the energies ofσ *and* σ^* NBO's and n_σ is the population of the donor σ orbital.

The occurrence of lone pair to σ^* interaction point to the charge transfer from anion to cation, apparent in N_{29}–H_{32}···O_{15}, N_{29}–H_{31}···O_{17}, N_{38}–H_{40}···O_{17}, N_{44}–H_{46}···O_{18}, N_{51}–H_{52}···O_{33}, N_{44}–H_{49}···O_{34}, N_{38}–H_{39}···O_{35} and N_{11}–H_{13}···O_{36} intermolecular hydrogen bonding interactions in GuLG molecule with interaction energies 14.39, 11.99, 8.44, 6.61, 9.64, 10.96, 8.14 and 2.73 kcal/mol, respectively. These interactions confirm the delocalization of charge in the cation moiety. The intramolecular hydrogen bonding

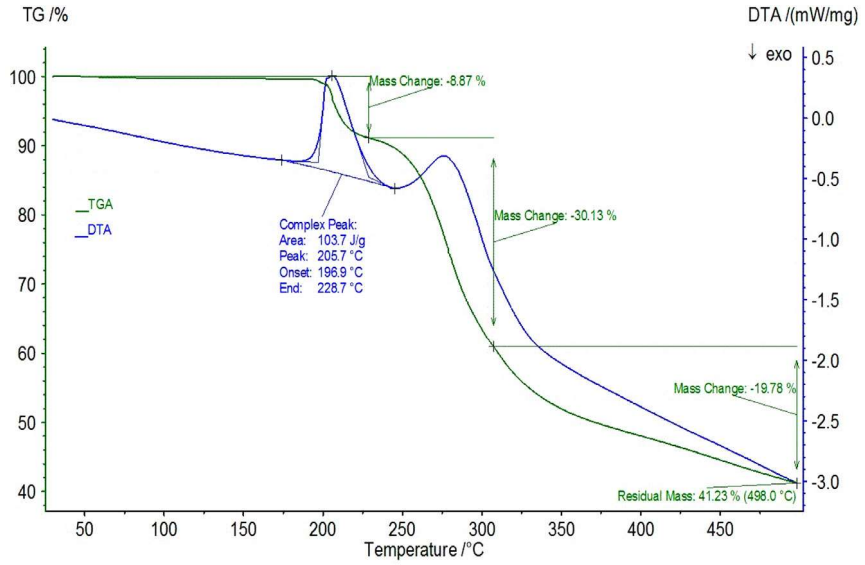

Fig. 6. TG-DTA thermogram of GuLG.

interaction in the L-glutamate anion in GuLG molecule manifests n1 (O_{17}) → $\sigma^*(N_{11}–H_{12})$ and n1 (O_{34}) → $\sigma^*(N_{29}–H_{30})$ having stabilization energies 12.92 and 4.23 kcal/mol, respectively. These intra- and intermolecular hydrogen bonging and charge transfer interactions enhance the NLO activity.

The natural population analysis (NPA) reveals that all carbon atoms are negative except C_1, C_{10}, C_{19}, C_{28},$C_{37}$and C_{47}; those are bonded with nitrogen and oxygen atoms. These carbon atoms become positive as they are attached to electronegative atoms which pull out the partial charges. C_{19}(0.8133 e) and O_{17} (0.8503 e) show the greatest amount of protonation and deprotonation respectively. C_{19} is surrounded by two oxygen atoms in the carboxylate part. All of the hydrogen atoms are seen to have positive values for atomic charges, in the range 0.2247e to 0.4685e, the largest of which are observed for H_{12}, H_{13}, H_{30}, H_{31}, H_{32}, H_{39}, H_{40}, H_{46}, $H_{49}$and H_{52}which are involved in hydrogen bonding (0.4641 e, 0.4993 e, 0.4606 e, 0.4727 e, 0.4786 e, 0.4559 e, 0.4468 e, 0.4598 e, 0.4685 e and 0.4667 e, respectively). The hydrogen bonding in the crystal is thus evident from this result, which is also concurrent with the results of NBO analysis.

4.6. Thermal analysis

The TG-DTA curves for GuLG are given in Fig. 6. The TG curve exhibits mass loss of the sample occurring at three temperature regimes. The first step of mass loss is seen between 478- 498 K with $\Delta m = 8.8\%$, which is explained as occurring because of the evaporation of water and to the release of NH_3. The area in DTA is the endothermic peak area which corresponds to the energy required for the first mass loss. The second and third instances of mass loss are observed between 508 and 598 K with $\Delta m = 30\%$, and 771 K with $\Delta m_{total} = 41\%$, which are explained as due to thermal decomposition of residual organic matter. The exothermic events in the DTA profiles point to the simultaneous occurrence of complete thermal decomposition and crystallization. DTA curves shows peaks at 478 K and 527 K . The first endothermic peak at 478 K corresponds to the melting point of the GuLG and the second endothermic peak at 527 K corresponds to the decomposition of the material. The good crystallinity of the grown crystal is revealed from the sharp endothermic peaks [42]. Complete decomposition of the sample at 771 K is also evident from the figure.

4.7. Linear optical spectral analysis

The experimental and simulated UV–Vis spectra of GuLG are shown in Fig. 7(a). The absorption peak at 191 nm is attributed to π-π^* electronic transition due to the carboxylate group in GuLG. Since there is no appreciable absorption in the visible region, the crystal can be considered for NLO and optoelectronic applications in the visible region and as window material in optical instruments [43]. The calculated (Table 2) absorption with maximum oscillator strength is found to be at 216 nm. This excitation gas phase has been forecasted in TD-DFT and the electronic absorption corresponds to the transition from the ground to the excited state which explained by the electron excitation from the HOMO to LUMO as well as the n→π^* transition takes place with 67% contribution.

The nonlinear capability of molecules, which prove to be of importance in the field of optoelectronics, is manifested in the high values of hyperpolarizabilities exhibited by them. Energy gap calculations are used to study about their chemical reactivity and kinetic stability. Soft molecules are ones in which the frontier orbital gap is small and hence are highly polarizable. They are usually re-

Table 2
UV–vis excitation energy and oscillator strength for GuLG calculated by TD-CAM-B3LYP.

Energy (cm^{-1})	Wavelength (nm)		Osc. Strength (f)	Symmetry	Major contributions
	Calc.	Exp.			
45,703	218		0.0001	Singlet-A	HOMO-4→LUMO+3 (68%), HOMO→LUMO (22%)
45,727	216		0.0057	Singlet-A	HOMO-2→LUMO (67%), HOMO-4→LUMO+5 (27%)
46,116	201	191	0.0012	Singlet-A	HOMO→LUMO (92%)

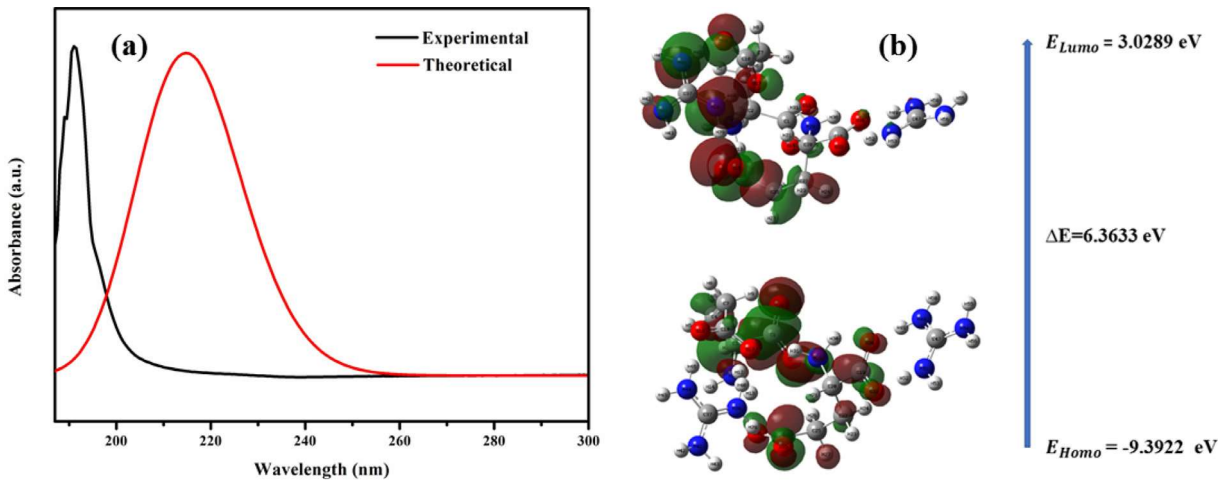

Fig. 7. (a): Electronic absorption spectra of GuLG (absorption wavelength λ(nm), excitation energies E (eV) and oscillator strengths (f)) using TD-DFT method and (b) HOMO-LUMO energy gap of GuLG.

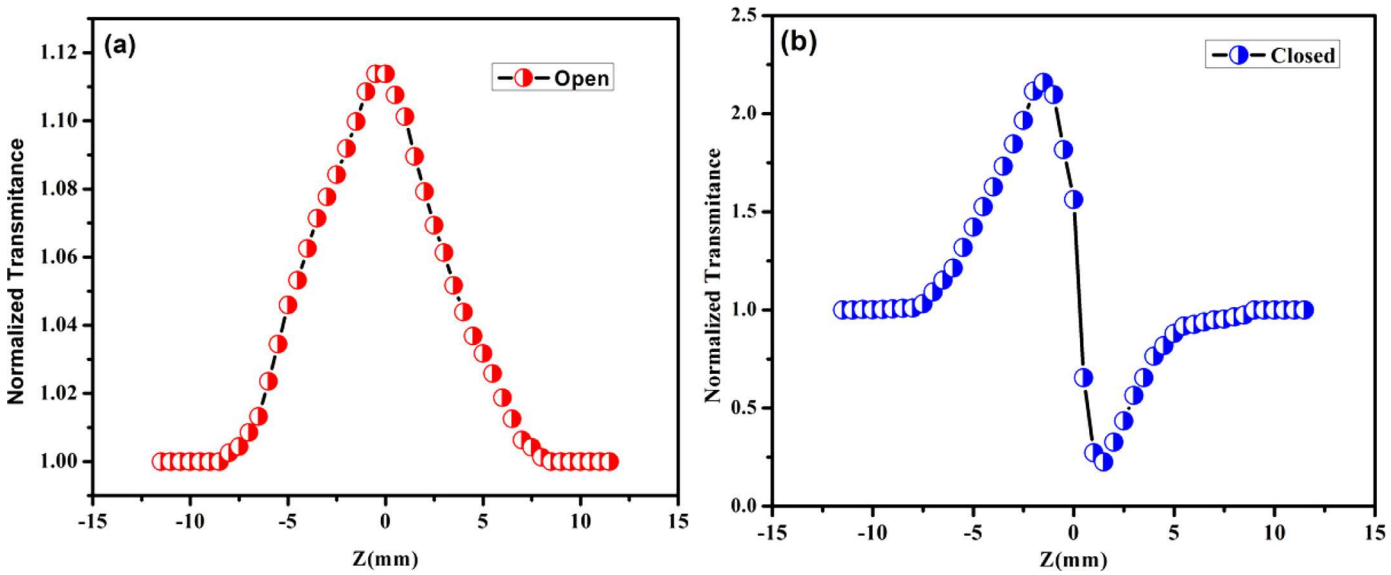

Fig. 8. (a) Open aperture and (b) Closed aperture traces of GuLG.

lated with high values of chemical reactivity and low values of kinetic stability. 3D plots of the frontier orbitals of GuLG are shown in Fig. 7b. From the figure, it is seen that HOMO is located on L-glutamate and the LUMO is found on delocalized guanidinium. These results show that HOMO acts as an electron donor and the LUMO ~~is~~ acts as the electron acceptor. HOMO and LUMO energies are −9.39228 eV and −3.0289 eV and the HOMO–LUMO gap value of the GuLG compound is 6.3633 eV. HOMO energy is associated directly with the ionization potential, LUMO energy is associated with the electron affinity. The LUMO transition and the low HOMO–LUMO energy gap account for the possibility of intramolecular charge transfer (ICT) taking place from electron-donor group to the acceptor group to form guanidinium L-glutamate charge transfer complex.

4.8. Third order nonlinear optical studies

The z-scan technique was employed to determine the NLO properties of GuLG, in which the sample was translated along the z-direction and the transmittance as a function of sample position was studied. The sample was dissolved in water–methanol (1:1)) and placed in a 1 mm path length glass cuvette. Laser beam from a diode-pumped Nd:YAG continuous wave laser ($\lambda = 532$ nm, $P = 50$ mW) was focused onto the sample solution making use of a 3.5 cm focal length lens. The intensities of the reference beam obtained from beam splitter and transmitted beams in closed aperture and open aperture modes were measured at the same time with the help of two detectors linked to power metre at different sample positions. The linear transmittance was maintained to be ~ 63%. The open and closed aperture z-scan curves are shown in Figs. 8(a) and 8(b). The open aperture z-scan curve is symmetric about the focus ($z = 0$), at which point it shows maximum transmittance, indicating saturable absorption (SA) taking place in the sample. The closed aperture pattern shows an asymmetric peak preceding a valley, which point to a negative refractive nonlinearity or self-defocusing effect, which is of thermo-optic origin. The self-defocusing effect is explained to be arising from local fluctuations of the refractive index with temperature. The normalized transmittance for the open-aperture (OA) and closed-aperture (CA) Z-scan mode is calculated using the following equation [44–46].

Third-order nonlinear parameters such as nonlinear absorption coefficient (β), nonlinear refractive index (n_2), third-order nonlinear optical susceptibility ($\chi^{(3)}$) and thermo-optic coefficient have been calculated and are presented in Table 3.

Table 3
Nonlinear optical parameters obtained from Z-scan measurement data for GuLG.

	n_2 x 10^{-8} cm^2/W	β x 10^{-4} cm/W	*Re* $\chi^{(3)}$ x 10^{-6} esu	Linear refractive index (n_0)	Im$\chi^{(3)}$ x 10^{-6}esu	$\chi^{(3)}$ x 10^{-6}esu	Limiting Threshold (mW)	Clamping value (mW)
GuLG	8.78	0.08	2.73	1.11	0.50	2.78	19.5	5.3

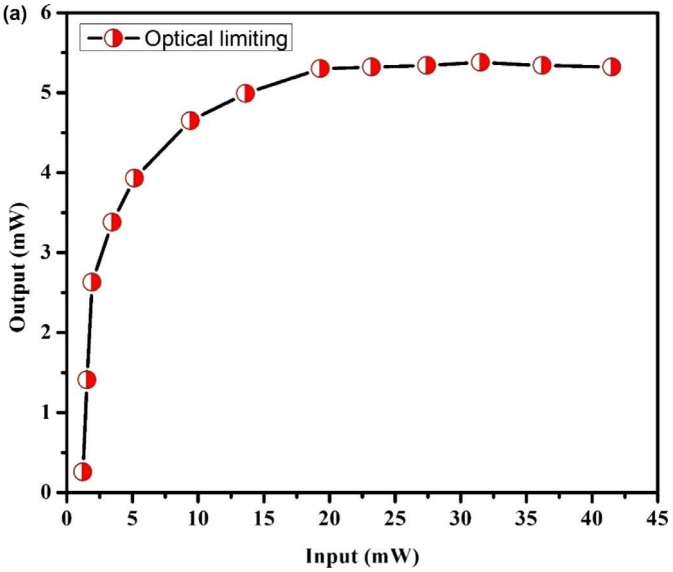

Fig. 9. Optical limiting pattern ofGuLG. (a) Experimental FT-IR spectra of GuLG and (b) Simulated Infrared spectra of GuLG.

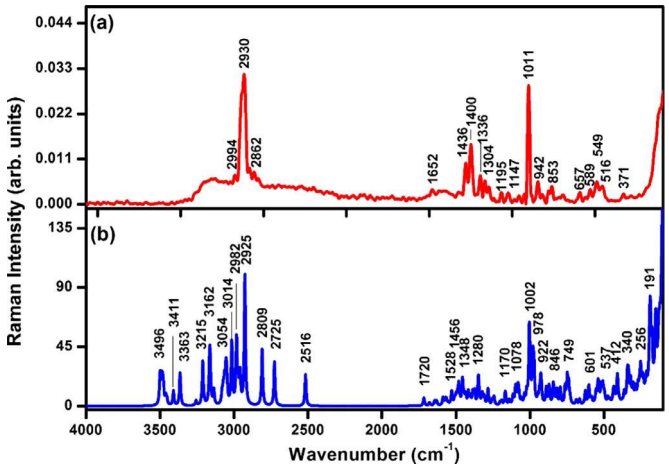

Fig. 10. (a) Experimental FT-Raman spectrum of GuLG and (b) Simulated Raman spectrum of GuLG.

The laser power at which the sample transmission is affected by its nonlinearity is determined to get an idea regarding the optical limiting behaviour of the sample. Thermally induced nonlinearity was due to temporal variations arising from linear and nonlinear absorption in medium. Laser heating results in the creation of an acoustic wave which affects the density of the medium, bringing about a change in refractive index. The optical limiting experiment was performed by placing the sample at the valley point and the output power was measured for various input powers of laser. The obtained characteristic curve is as shown in Fig. 9. From the optical limiting curve, the transmitted output intensity is seen to show a linear variation with very low input intensities, but a deviation from the linear behaviour is seen at high incident intensities. At still higher input powers, the output intensity curve shows a characteristic plateau which saturates at the limiting amplitude. The sample exhibits low limiting amplitude which points to its good limiting behaviour. The values of nonlinear refractive index, nonlinear absorption coefficient and third order nonlinear optical susceptibility are obtained to be 6.40 × 10^8 cm^2 /W, 0.32 × 10^4 cm/W and 2.65 × 10^6 esu respectively in L-Glutamic acid hydrochloride [50], and 5.34 × 10^{-8} cm^2/W, 0.03 × 10−4 cm/W, and 1.47 × 10^{-6} esu respectively in guanidinium 4-aminobenzoate [54], under similar excitation conditions. The above results show that GuLG can be used for optical limiting applications under nanosecond excitation.

The static and dynamic dependant nonlinear parameters viz. static first-hyperpolarizability $\beta(0;\ 0,\ 0)$, static-second-hyperpolarizability $\gamma(0;\ 0,\ 0,\ 0)$, electro-optical Pockels effect $\beta(-\omega;\omega,0)$, second-harmonic generation $\beta(-2\omega;\omega,\omega)$, dynamic second-hyperpolarizabilities for the quadratic electro optic Kerr effect $\gamma(-\omega;\omega,0,0)$, and electric-field-induced second harmonic generation $\gamma(-2\omega;\omega,\omega,0)$ for GuLG were calculated using the CAM-B3LYP /6–311++g(d,p) method and are presented in Table 4. The dynamic dependence of hyperpolarizability was estimated at the 1064 nm ($\hbar\omega = 0.042823\ a.u$) wavelength of Nd: YAG laser.

4.9. Vibrational spectral analysis

The analysis of vibrational spectra has been carried out based on the FT-IR and FT-Raman spectra along with the vibrational wavenumbers computed at the B3LYP 6–31++G(d) level. The observed and simulated spectra of GuLG molecule are shown in Fig. 9 and Fig. 10 for visual comparison. The observed and calculated wavenumbers along with the vibrational assignments with Potential energy distribution (PED) of the GuLG are given in Table 5. The absence of negative wavenumbers for the stationary points on the molecular potential energy surface establishes that this structure corresponds to real minimum. The vibrational spectral assignments have been carried out on the basis of characteristic vibrations of guanidinium cations and L-glutamate anions. The detailed analysis of vibrational wavenumbers of GuLG is discussed below.

Table 4
Comparison of static and field dependant first & second hyperpolarizability, polarizability, and dipole moment for the GuLG and Urea molecules are calculated with CAM-B3LYP / 6–31++G(d,p).

NLO properties	GuLG	Urea	NLO properties	GuLG	Urea
$\beta(0;0,0)(\times10^{-30}esu)$	4.140	0.762	$\alpha(0;0)\langle\alpha\rangle(\times10^{-24}\ esu)$	31.791	4.967
$\beta(-\omega;\omega,0)(\times10^{-30}esu)$	5.992	0.932	$\alpha(-\omega;\omega)\langle\alpha\rangle(\times10^{-24}\ esu)$	32.831	5.029
$\beta(-2\omega;\omega,\omega)(\times10^{-30}esu)$	10.921	1.75	$\alpha(0;0)\Delta\alpha(\times10^{-24}\ esu)$	8.824	0.736
$\gamma(0;0,0,0)(\times10^{-36}esu)$	17.370	4.036	$\alpha(-\omega;\omega)\Delta\alpha(\times10^{-24}\ esu)$	32.831	0.7409
$\gamma(-2\omega;\omega,\omega,0)(\times10^{-36}esu)$	68.514	7.820	$\mu_{total}(Debye)$	13.533	3.826
$\gamma(-\omega;\omega,0,0)(\times10^{-36}esu)$	23.035	5.357			

Table 5
Experimental FT-IR, Raman and theoretical wavenumbers in (cm^{-1}) assignments and PED contributions of GuLG crystal by NCA based on SQM force field calculations.

ν_{cal} (cm^{-1}) scaled	ν_{IR} (cm^{-1})	ν_{Raman} (cm^{-1})	IR Intensity	Raman Intensity	Assignment with PED[a] (%)
3409	3374 sbr	–	1.046	35.97	$\nu_{as}NH_2$ (86)
3256	3207 br	–	5.489	8.934	ν_{as} NH_3^+ (89)
3136	–	3126 br	31.01	35.57	$\nu_sNH_3^+$ (77)
3048	3042 br	–	0.001	13.3	ν_s NH_3^+ (65)
3015	–	2994 m	0.724	23.95	ν_sNH_2 (59), ν_{as} CH_2 (28)
2959	–	2930 vs	0.626	16.91	ν_s CH_2 (97)
2926	–	2896 m	11.41	21.71	ν_sNH_2 (78)
1680	1681 vs	1652 m	9.569	0.008	δ NH_2 (57)
1631	1622 s	–	1.848	0.382	ν $C=O$ (80)
1588	1580 s	1590 w	1.627	0.086	ν $C=N$ (65), ν CC (21)
1509	–	1484 w	6.831	0.25	δ NH_3^+ (57)
1480	1482 m	–	7.577	0.024	δ CH_2 (75)
1437	–	1436 s	0.056	0.279	δCH_2 (37)
1412	1407 s	1400 s	3.216	0.098	ρ CH_2 (29)
1350	1338 m	1356 m	2.232	0.18	ν CO (58)
1309	1295 m	1304 m	0.271	0.052	ν CC (68), ρ NH_2 (25)
1283	–	1277 w	0.336	0.063	δ CCH (37)
1191	1190 w	1195 m	0.932	0.05	δHCC(50)
1141	1151 m	1147 w	0.42	0.054	ρ NH_3^+ (42), γ CH_2 (24)
1114	–	1110 w	0.506	0.011	ρ NH_2 (23)
1094	1075 m	1074 w	1.161	0.011	ν CC (35), ν CN (23)
1036	1039 m	1037 w	2.534	0.014	δ CNH (60)
1004	–	1011vvs	0.785	0.148	ν CC(40), ρ NH_3^+ (15),
999	989 w	989 w	1.112	0.009	τ CONH (19)
975	964 w	–	0.898	0.058	ν CN(59)
947	–	946 m	0.876	0.014	ν CN (30), δCH2 (20),
923	913 w	918 w	0.649	0.029	ν CC (39)
871	869 w	853 w	0.094	0.038	ν CC (22)
834	827 w	821 w	2.918	0.005	δ NHO (35)
819	805 w	797 w	1.133	0.006	τ CCO (23),
763	–	776 w	0.256	0.031	τ CCO(32)
665	668 w	657 m	0.89	0.006	δ COO (45)
626	632 w	624 w	0.493	0.004	γ CC (34), δ COO (24)
583	582 w	587 w	1.101	0.004	γ CC (25)
554	–	549 m	2.609	0.005	τ CNC (12)
538	523 w	516 w	4.266	0.002	γ CN (46)
363	–	371 w	0.364	0.001	δ NH···O (26)
320	–	320 w	0.494	0.001	τ NCN (21)
89	–	92 s	0.171	0.001	τ NH···O (35)
76	–	75 s	0.022	0.001	τ CO···H (37)

υ: stretching, γ: scissoring, ω: wagging, τ: torsion, Γ: twisting, β: in-plane bending, δ: deformation, ρ:rocking, s: symmetric, as: antisymmetric, vs:very strong, s: strong, ms: medium strong, w: weak.

4.9.1. Vibrations of guanidinium cations

The stretching vibrations of NH_2 group in guanidinium group typically occurs in the range 3500–3300 cm^{-1} [47,48]. The PED shows the contribution from the asymmetric stretching vibration of the non-hydrogen bonded NH_2 group at 3409 cm^{-1} as well as the non-hydrogen bonded NH_2 asymmetric stretching mode observed at 3373 cm^{-1}in IR spectrum. But the presence of hydrogen bonding interactions with the carboxylate group of L-glutamate, the NH_2 symmetric stretching modes of guanidinium are found to be red shifted to 2994 cm^{-1} and 2896 cm^{-1} (medium bands) in the Raman spectrum. The DFT calculations support the existence of hydrogen bonding in the GuLG molecule and predict NH_2 stretching mode at 3015 cm^{-1} and 2926cm^{-1} with PED contributions of 59% and 78% for the modes. The transfer of electrons from the lone pair of electron donor to the σ^*(N–H) of electron acceptor stretches the N–H bond and leads result in N–H···O red-shifted hydrogen bonds. NBO analysis and stabilized geometry clearly support these results which enhance the NLO activity.

NH_2 bending vibrations δ (NH_2) are characterised by high wavenumber and high intensity [49]. In GuLG molecule, the very intense band at 1681 cm^{-1}in IR and the medium band at 1652 cm^{-1}in the Raman spectrum, is due to NH2 scissoring mode, while the computed wavenumber is 1680 $cm^{-1}$with 57% PED contribution. The rocking deformation vibrations of NH_2 group are usually observed in the region 1150–1100 cm^{-1}. A weak band absorption band observed in Raman spectrum at 1110 $cm^{-1}$is attributed to the rocking vibration of NH_2 group of guanidinium cation (23% PED). Guanidines show strong absorption at 1685- 1580 cm^{-1} due

to C = N stretching vibrations [49]. This is manifested in GuLG as a strong absorption band seen at 1580 cm^{-1}in IR and a weak absorption band at 1590 cm^{-1}in Raman spectra (65% PED) coupled with the 21% PED contribution of C–C stretching in L-glutamate anion.

4.9.2. Vibrations of L-glutamate anion

The asymmetric and symmetric stretching vibrations of NH_3 occur in saturated amines in the region 3380–3350 cm^{-1} and 3310–3280 cm^{-1}, respectively [50–53]. In GuLG, asymmetric stretching mode of NH_3^+ group is observed as a weak and broad band at 3207 cm^{-1}in IR spectrum. NH_3^+symmetric stretching vibrational mode is observed as broad bands at 3126 cm^{-1} (77% PED) in Raman and 3042 cm^{-1} in IR (65% PED). In additon, the position and broadness of the NH_3^+ symmetric and asymmetric stretching modes and the protonation of NH_3^+group with shift of wavenumber suggest the presence of strong N–H···O intermolecular hydrogen bonds. This hydrogen bonding interaction leads to the charge transfer in GuLG, thereby making it NLO active. DFT calculations show that L-glutamate cations are connected with the guanidinium anions through N–H···O hydrogen bonds. This also points to the strong hydrogen bonding between hydrogen and oxygen, giving noncentrosymmetry to the GuLG crystal, thus enhancing its molecular hyperpolarizability.

The CH_2 asymmetric and symmetric stretching vibrations normally appear in the region 2936 ± 20 cm^{-1} and 2863 ± 20 cm^{-1}, respectively [52,53]. CH_2 symmetric stretching is seen at 2930 cm^{-1} (very strong) in GuLG, with 97% PED contribution. In symmetric CH_2 stretch, the blue-shifted wavenumber shows the formation of C–H···O intramolecular hydrogen bonding of CH_2 group with a carboxylate group. Scissoring vibration of CH_2 is observed as medium and strong bands in IR (1482 cm^{-1}) and Raman (1436 cm^{-1}) spectra, respectively. NH_3^+ and CH_2 bending vibrations are presented in Table 5 C–N and C–C skeletal vibrations are commonly expected at 1150–850cm^{-1} [53]. In GuLG, C–C stretching is attributed to the peaks obtained at 1075 cm^{-1} (IR), 913 cm^{-1} (IR), 869 cm^{-1}(IR), 1074 cm^{-1} (Raman), 1011 cm^{-1}(Raman), 918 cm^{-1}(Raman) and 853cm^{-1}(Raman). C–N stretching mode is seen at 964 cm^{-1}in IR and 946 cm^{-1}in Raman.

5. Conclusions

Single crystals of GuLG have been grown by slow evaporation of solution method. The vibrational spectra have been recorded experimentally using FT-IR and FT-Raman methods and analysed with the aid of DFT methods. N–H ....O hydrogen bonding interaction in GuLG is confirmed from the red-shifting of NH stretching wavenumbers. NBO analysis predicted the intramolecular hydrogen bonding interaction in the L-glutamate anion in GuLG molecule, manifested in n1 (O_{17}) → $\sigma^*(N_{11}–H_{12})$ and n1 (O_{34}) → $\sigma^*(N_{29}–H_{30})$ having stabilization energies 12.92 and 4.23 kcal/mol, respectively. These intra and inter molecular hydrogen bonding and charge transfer interactions enhance the NLO activity. The π-π^* transitions due to carboxylic group give rise to the electronic absorption maximum for solution phases of GuLG. The low HOMO–LUMO energy gap account for the possibility of intramolecular charge transfer which contributes to the NLO activity in GuLG. The theoretically predicted values for electronic NLO response contributions of the molecule have showed their better NLO property compared to urea molecule. The open-aperture Z-scan study suggests the potentiality of the material in optical limiting applications.

Authorship contribution statement

Author contributions Specific contributions made by each author have been given below:

Rejeena V. Rajan: Conceptualization, Methodology, original draft writing

Merin George: Preparation of the sample, draft writing - review & editing

D. R. Leenaraj: Conceptualization

Reena Ittyachan: Preparation of the sample

D. Sajan: Conceptualization, Methodology, Funding acquisition, Supervision, Project administration

G. Vinitha: Facility provided and Supervision of Z-scan measurement

Declaration of Competing Interest

The authors declare that they have no known competing financial interests or personal relationships that could have appeared to influence the work reported in this paper.

Acknowledgments

D.Sajan (DS) thanks the UGC-DAE Consortium for Scientific Research, Mumbai Centre, R-5 Shed, Bhabha Atomic Research Centre, Trombay, Mumbai 400085 INDIA for the financial support (U DCSR/MUM/CD/CRS-M-238/2017/1007 dt.16.01.2017). The authors (DS and MG) also acknowledge the DST-FIST program (SR/FST/College-182/2013, November 2013 & FIST No.393 dated 25-09–2014) to the Bishop Moore College Mavelikara for providing the UV visible and Computational facilities. The author (DS) is highly grateful to Prof. T. Sundius for the Molvib program and fruitful discussions on the Normal Coordinate Analysis (NCA).

Supplementary materials

Supplementary material associated with this article can be found, in the online version, at doi:10.1016/j.molstruc.2020.128937.

References

[1] V.G. Dmitriev, G.G. Gurzadyan, D.N. Nicogosyan, Handbook of Nonlinear Optical Crystals, Springer-Verlag, New York, 1999.
[2] E. Ishow, C. Bellaïche, L. Bouteiller, K. Nakatani, J.A. Delaire, J. Am. Chem. Soc. 125 (2003) 15744.
[3] M.S. Wong, C. Bosshard, F. Pan, P. Gunder, Adv. Mater. 8 (1996) 677.
[4] L.R. Dalton, P.A. Sullivan, B.C. Olbricht, D.H. Bale, J. Takayesu, S. Hammond, H. Rommel, B.H. Robinson, Tutorials in Complex Photonic Media, SPIE, Bellingham, WA, 2007.
[5] X. Liu, X. Wang, X. Yin, S. Liu, W. He, L. Zhu, G. Zhang, D. Xu, CrystEngComm 16 (2014) 930.
[6] W. Zhang, X. Tao, C. Zhang, H. Zhang, M. Jiang, Cryst. Growth Des. 9 (2009) 2633.
[7] L. Kang, Z. Lin, J. Qin, C. Chen, Sci. Rep. 3 (2013) 1366.
[8] H.J. Zhao, Y.F. Zhang, L. Chen, J. Am. Chem. Soc. 134 (2012) 1993–1995.
[9] D. Yuan, Z. Jia, J. Wang, Z. Gao, J. Zhang, X. Fu, J. Shu, Y. Yin, Q. Hu, X. Tao, CrystEngComm 16 (2014) 4008.
[10] W. Zhang, R.-.G. Xiong, Chem. Rev. 112 (2011) 1163.
[11] H. Zhao, Z.-.R. Qu, H.-.Y. Ye, R.-.G. Xiong, Chem. Soc. Rev. 37 (2008) 84.
[12] Z. Sun, S. Li, S. Zhang, F. Deng, M. Hong, J. Luo, Adv. Opt. Mater 2 (2014) 1199.
[13] R. Mohan Kumar, D. RajanBabu, G. Ravi, R. Jayavel, J. Cryst. Growth 250 (2003) 113.
[14] S.R. Marder, J.W. Perry, W.P. Schaefer, Science 245 (1989) 626.
[15] V. Venkataraman, G. Dhanraj, V.K. Wadhawan, J.N. Sherwood, H.L. Bhat, J. Cryst. Growth 154 (1995) 92.
[16] S. Nandhini, P. Murugakoothan, Material Lett 241 (2019) 152–155.
[17] S. Nandhini, S. Muniyappan, Venkadesh kumar Ramar, Karthikeyan Balasubramanian, P. Murugakoothan, J.Mol.Struct 1198 (2019) 126859 Materials Letters.
[18] J.M. Adams, R.W.H. Small, ActaCryst. B 32 (1976) 832–835.
[19] V. Suvitha, P. Vivek, P. Murugakoothan, Optik (Stuttg) 124 (2013) 3534–3538.
[20] A. Suvitha, V. Sathyanarayanamoorthi, P. Murugakoothan, Spectrochim. Acta Part A: Mol. Biomol. Spectrosc 110 (2013) 255–261.
[21] B. Deepa, P. Philominathan, Optik (Stuttg) 127 (2016) 1507–1510.
[22] P. Arumanayagam, S. Ananth, P. Murugakoothan, Spectrochim. Acta Part A: Mol. Biomol. Spectrosc 97 (2012) 741–745.
[23] V. Sivashankar, R. Siddheswaran, T. Bharthasarathi, P. Murugakoothan, J. Cryst. Growth 311 (2009) 2709–2713.
[24] V. Sivashankar, R. Siddheswaran, P. Murugakoothan, Mater. Chem. Phys 130 (2011) 323–326.

[25] V. Siva, S. Suresh Kumar, A. Shameem, M. Raja, S. Athimoolam, S. AsathBahadur, J. Mater. Sci.: Mater. Electron 28 (2017) 12484–12496.
[26] Siva Vadivel, Asath Bahadur Sultan, Shameem Abdul Samad, Athimoolam Shunmuganarayanan, Raja Muthu, Chem. Phys. Lett 707 (2018) 165–171.
[27] B. Peng, Q. Peng, W. Zhou, Z. Zhou, Acta Crystallogr. E 66 (2010) o2679 o2679.
[28] M.J. Frisch, G.W. Trucks, H.B. Schlegel, G.E. Scuseria, M.A. Robb, J.R. Cheeseman, G. Scalmani, V. Barone, B. Mennucci, G.A. Petersson, H. Nakatsuji, M. Caricato, X. Li, H.P. Hratchian, A.F. Izmaylov, J. Bloino, G. Zheng, J.L. Sonnenberg, M. Hada, M. Ehara, K. Toyota, R. Fukuda, J. Hasegawa, M. Ishida, T. Nakajima, Y. Honda, O. Kitao, H. Nakai, T. Vreven, J.A. Montgomery Jr., J.E. Peralta, F. Ogliaro, M. Bearpark, J.J. Heyd, E. Brothers, K.N. Kudin, V.N. Staroverov, R. Kobayashi, J. Normand, K. Raghavachari, A. Rendell, J.C. Burant, S.S. Iyengar, J. Tomasi, M. Cossi, N. Rega, J.M. Millam, M. Klene, J.E. Knox, J.B. Cross, V. Bakken, C. Adamo, J. Jaramillo, R. Gomperts, R.E. Stratmann, O. Yazyev, A.J. Austin, R. Cammi, C. Pomelli, J.W. Ochterski, R.L. Martin, K. Morokuma, V.G. Zakrzewski, G.A. Voth, P. Salvador, J.J. Dannenberg, S. Dapprich, A.D. Daniels, O. Farkas, J.B. Foresman, J.V. Ortiz, J. Cioslowski, D.J. Fox, Gaussian 09, Revision A.1, Gaussian, Inc., Wallingford CT, 2009.
[29] A.D. Becke, J. Chem. Phys 98 (1993) 5648 5642.
[30] A.D. Becke, Phys. Rev. A 38 (1988) 3098–3100.
[31] C. Lee, W. Yang, R.G. Parr, Phys. Rev. B 37 (1988) 785–789.
[32] T. Sundius, J. Mol. Struct 218 (1990) 321.
[33] T. Sundius, Vib. Spectrosc 29 (2002) 89.
[34] E.D. Glendening, A.E. Reed, J.E. Carpenter, F. Weinhold, NBO Version 3.1, Theoretical Chemistry Institute and Department of Chemistry, University of Wisconsin, Madison, 1998.
[35] M.J. Turner, J.J. McKinnon, S.K. Wolff, D.J. Grimwood, P.R. Spackman, D. Jayatilaka, M.A. Spackman, CrystalExplorer17.5, University of WesternAustralia, 2017.
[36] , MERCURY 3.8, Cambridge Crystallographic Data centre, CCDC Software Limited, Cambridge, UK, 2010.
[37] H.O. Kalinowski, S. Berger, S. Braun, Carbon-13 NMR Spectroscopy, John Wiley&; Sons, Chichester, 1988.
[38] K. Pihlaja, E. Kleinpeter (Eds.), Carbon-13 Chemical Shifts in Structural andsterochemical Analysis, VCH Publishers, Deerfield Beach, 1994.
[39] M.A. Spackman, P.G. Byrom, Chem. Phys. Lett 267 (1997) 215–220.
[40] M.A. Spackman, D. Jayatilaka, CrystEng Comm. 11 (2009) 19–32.
[41] A.E. Reed, R.B. Weinstock, F. Weinhold, Natural population analysis, J. Chem. Phys.B 83 (1985) 735–746.
[42] V. Sivashankar, P. Murugakoothan, Mater. Chem. Phys 130 (2011) 323–326.
[43] M. Parthasarathy, R. Gopalakrishnan, Opt. Mater. 35 (2013) 2056–2061.
[44] M. Sheik Bahae, D.J. Hagan, IEEE LEOS Newsl 17 (2007).
[45] Y.S. Zhou, E.S. Wang, J. Peng, J. Liu, C.W. Hu, R.D. Huang, X. You, Polyhedron 18 (1999) 1419–1423.
[46] M.T. Zhao, B.P. Singh, P.N. Prasad, J. Chem. Phys 89 (1998) 5535.
[47] M. Drozd, J. Mol. Struct. (Thoechem) 756 (2005) 173–184.
[48] V. Sasikala, D. Sajan, K. Job Sabu, T. Arumanayagam, P. Murugakoothan, Spectrochim. Acta Part A 139 (2015) 555–572.
[49] M. Drozd, J. Baran, Spectrochim. Acta Part A 61 (2005) 2953–2965.
[50] Lija K. Joy, Merin George, Javeesh Alex, Arun Aravind, D. Sajan, G. V.initha, J.Mol. Struct. 1156 (2018) 733–744.
[51] D.L. Vein, N.B. Colthup, W.G. Fateley, J.G. Grasselli, The Handbook of Infraredand Raman Characteristic Frequencies of Organic Molecules, Academic Press, New York, 1991.
[52] H. Ratajczak, J. Baran, J. Barycki, S. Debrus, M. May, A. Pietraszko, H.M. Ratajczak, A. Tramer, J. Venturini, J.Mol. Struct 555 (2000) 149.
[53] S. Debrus, H. Ratajczak, J. Venturini, N. Pincon, J. Baran, J. Barycki, T. Glowiak, A. Pietraszko, Synth. Met 127 (2002) 99.
[54] Jesby George, V. Sasikala, Lija K. Joy, D. Sajan, T. Arumanayagam, P. Murugakoothan, G. Vinitha, Opt Mater (Amst) 89 (2019) 48–62.

0022-2860
ISSN